PCCP

Accepted Manuscript

ROYAL SOCIETY OF CHEMISTRY

www.rsc.org/pccp

Effects of Thermal Disorder on Electronic Properties of Ordered Polymers

Marko Mladenović,[a,b] **and Nenad Vukmirović**[*a]

Received Xth XXXXXXXXXX 20XX, Accepted Xth XXXXXXXXX 20XX
First published on the web Xth XXXXXXXXXX 200X
DOI: 10.1039/b000000x

The effects of thermal disorder on electronic properties of crystalline polymers were investigated. Atomic configurations of the material were obtained using classical Monte Carlo simulations at room temperature, while electronic structure calculations were performed using density functional theory based charge patching method and overlapping fragments method. We investigated two different stable configurations of crystalline poly(3-hexylthiophene) (P3HT) and calculated the density of electronic states and the wave function localisation. We found that the effect of disorder in side chains is more pronounced in the more stable configuration of P3HT than in the other one due to larger conformational freedom of side chains. The results show that disorder in main chains has strong effect on the electronic structure and leads to the localisation of the wave functions of the highest states in the valence band, similar to localisation that occurs in amorphous polymers. The presence of such states is one possible origin of thermally activated electrical transport in ordered polymers at room temperature.

1 Introduction

Materials based on conjugated polymers attract a lot of interest due to their applications in electronic devices such as organic field-effect transistors, organic light-emitting diodes and organic solar cells.[1–5] These materials contain both crystalline and amorphous regions and consequently their electronic properties strongly depend on their morphology. In crystalline regions of the material, thiophene rings are connected into main (backbone) polymer chains, which then form two dimensional lamellar structures separated by insulating side chains.

Crystalline polymer regions exhibit better transport characteristics than amorphous regions. At first, one may expect that the electronic states in crystalline regions are fully delocalised due to the effect of periodicity. On the other hand, wave functions of electronic states in amorphous regions are well localised due to the effects of disorder. Calculations of the electronic structure of amorphous polymers show that wave functions of the highest states in the valence band are localised on few rings only.[6,7] The electronic states in crystalline regions may also exhibit localisation due to the effects of thermal disorder; at finite temperature the atoms are displaced from their equilibrium positions in a random manner and the atomic positions no longer exhibit periodicity. The importance of the effects of thermal (or dynamic, which is an alternative expression often used in the literature) disorder in small molecule based organic crystals is now widely recognized.[8–14] On the other hand, the effects of thermal disorder in polymers are less well understood. Currently available simulation results[15–17] suggest that the highest valence band states in ordered polymer materials at room temperature are localised. However, most of these calculations either consider a single polymer chain or do not include the effects of side chains.

The aim of this work is to investigate in detail the effects of thermal disorder on electronic properties of ordered polymer materials and to identify relative importance of various sources of thermal disorder. For concreteness, we choose poly(3-hexylthiophene) (P3HT) polymer for our study. We calculate the electronic density of states (DOS) and the localisation of hole wave functions. Atomic configurations at finite temperature are obtained using Monte Carlo (MC)[18] simulations, while the charge patching method (CPM)[6,7,19,20] and the overlapping fragments method (OFM)[7,21] are used for electronic structure calculations.

The disorder in the structure at finite temperature comes both from the disorder in the shape of the flexible alkyl side chains (that will be referred to as side chain disorder from now on) and from the disorder due to variations of torsion angles between thiophene rings in the main chains and the position of main chains (that will be referred to as main chain disorder from now on).[22] One should note that disorder of main or side chains does not imply an amorphous material. While it is well known that the wave functions in conjugated polymers are localised on the main chain, side chains with a disordered shape still affect the electronic structure as they create a disor-

[a] *Scientific Computing Laboratory, Institute of Physics Belgrade, University of Belgrade, Pregrevica 118, 11080 Belgrade, Serbia, E-mail: nenad.vukmirovic@ipb.ac.rs*
[b] *School of Electrical Engineering, University of Belgrade, P.O. Box 35-54, 11120 Belgrade, Serbia*

dered electrostatic potential on the main chain. Disorder in the shape of the main chain mostly affects the electronic structure through variations in electronic coupling between the rings. To isolate the effects of main and side chain disorder we investigate three types of structures: (1) the structures with straight main chains and disordered alkyl side chains; (2) the structures with disordered main chains in the absence of side chains; (3) the structures with both main and side chains disordered.

We find that the effects of disorder are least pronounced in the structures with disordered side chains. Strong wave function localisation of highest valence band states occurs in structures with main chains disordered, both with and without side chains. Such a localisation is one possible origin of thermally activated transport observed in all reported P3HT mobility measurements.

2 Methods for atomic and electronic structure calculations

The method used for electronic structure calculations is schematically described in Fig. 1. The atomic structure is obtained using in-house delevoped Monte Carlo (MC) simulations. It is subsequently used to calculate the electronic structure, using the CPM and the OFM.

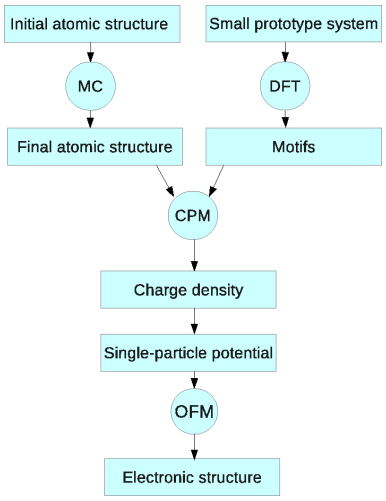

Fig. 1 Schematic representation of the algorithm for the electronic structure calculations.

2.1 Lattice constants

The initial structure for MC simulations is the ideal crystalline structure of P3HT. Atomic structure of crystalline P3HT was extensively studied and different possible configurations were found.[23–32] Two different stable crystalline structures are simulated at 300 K: aligned and shifted, which are shown in Fig 2. In the aligned structure, thiophene rings from two adjacent main chains in the π-π stacking direction are aligned. On the other hand, in the shifted structure, thiophene rings from two adjacent chains in the π-π stacking direction are mutually shifted by the half of the unit cell in the main chain direction. Parameters of the unit cells are found using NPT (constant pressure and temperature) MC simulation at 300 K and 101.325 kPa. During the simulation, the size of the box in the main chain direction is kept constant, while two other dimensions are changed. The energy of the system is modelled as a sum of the long-range (van der Waals and Coulomb) interactions between atoms from different chains. Expression and parameters for the long-range interactions are taken from the OPLS parameters set,[33] which was previously successfully applied for the simulations of the same material.[15] Cutoff for these interactions is taken to be 12 Å. The unit cell parameters are determined as the parameters obtained when the system reaches thermal equilibrium. For the aligned structure these are: $a/2 = 15.7$ Å, $b = 8.2$ Å and $c = 7.77$ Å , while for the shifted structure these are: $a/2 = 15.7$ Å, $b = 8.1$ Å and $c = 7.77$ Å. All unit cell angles are taken to be 90°. These parameters are in very good agreement with previous computational results for the same structures of P3HT. For example, the unit cell parameters obtained for the aligned structure in Ref. 24 are: $a/2 = 16$ Å, $b = 8.2$ Å and $c = 7.81$ Å, while for the shifted these are: $a/2 = 16$ Å, $b = 7.85$ Å and $c = 7.81$ Å. On the other hand, experimental results based on the X-ray diffraction measurements suggest somewhat higher value for the side chains stacking direction of 16.8 Å.[29] This difference might originate from the assumption of the ideal crystal structure without disorder made in the calculations, which is not the case in reality. Interdigitation between side chains from different lamellas is weaker in more disordered structures, and consequently, the unit cell parameter for the side chains stacking direction is higher. We find that the shifted structure is more stable at 300 K, since its potential energy per number of rings is 0.38 eV lower than the corresponding energy in the aligned structure, confirming the result given in Ref. 24 that the shifted structure is more energetically favourable.

2.2 Atomic structure

With the initial structure at hand, MC simulations are performed to obtain the snapshots of the atomic structure at room temperature. During the MC simulations bond lengths and bond angles are kept constant, while some or all torsion angles are changed. Variations of torsion angles affect electronic coupling between orbitals more strongly than variations of bond lengths and bond angles. For example, the thermal energy at room temperature $k_BT = 25$ meV leads to displacement of an

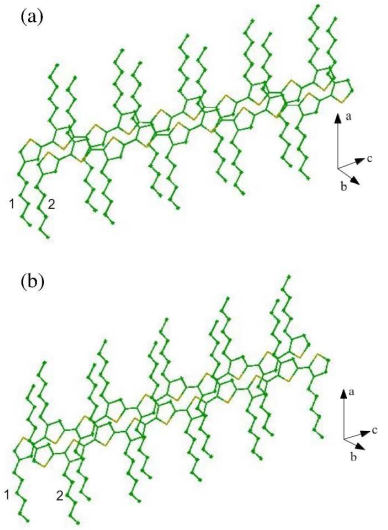

Fig. 2 Two stable configurations of crystalline P3HT: (a) aligned and (b) shifted. The main chain direction is denoted by *c*, the π-π stacking direction by *b* and the side chains direction by *a*.

atom due to bond stretching on the order of 0.02 Å , while the same energy leads to interring torsion angle change on the order of 45°, which yields the atomic displacements of more than 1 Å. For this reason, it is reasonable to keep bond angles and bond lengths constant. In each step of the MC simulation a new configuration is generated by changing the torsion angles and moving the whole polymer chain. The new configuration is accepted if it satisfies the Metropolis condition.[18] The energy of the system is calculated as a sum of torsion potentials and long range van der Waals and Coulomb interactions. Thiophene - thiophene torsion potential is taken from Ref. 6, while thiophene - side chain torsion potential is taken from Ref. 24. Long-range interactions are modelled in a same way as for lattice constants calculations. OPLS parameters set is also used for the torsion potentials within side chains. Periodic boundary conditions are applied in each direction of the unit cell for the systems with disorder in side chains. Boundary conditions are open in the main chain direction for the systems with disorder in main chains. The final atomic structure is taken after the system is thermally equilibrated at 300 K, which is evidenced from the saturation in the dependence of potential energy on the number of MC steps.

2.3 Electronic structure

The final atomic configuration obtained from MC simulations is used as input for electronic structure calculations. For the system containing more than thousand atoms density functional theory (DFT) calculations would be too computationally demanding. Therefore, CPM is applied instead of DFT. The main idea of the CPM is to calculate the electronic charge density directly, instead of obtaining it from self-consistent solving of Kohn-Sham DFT equations. The charge density is calculated as a sum of contributions (called motifs) of all atoms in the system. Motifs are extracted from the DFT calculations of a small prototype system containing 3 neighbouring rings of P3HT and they are the same as used in Ref. 6. CPM was previously applied to calculate the electronic structure of amorphous P3HT.[6,7] The details of the CPM are presented in Ref. 19.

When electronic charge density is obtained, the single-particle Kohn-Sham Hamiltonian is constructed by solving the Poisson equation for the Hartree potential and using the local density approximation (LDA) for the exchange-correlation potential.[34] The single particle Hamiltonian is then diagonalized using OFM. This method uses the eigenstates of small fragments of the system as the basis set. In this case, fragments are systems of 3 neighbouring rings of P3HT (trimers). In previous work we demonstrated that a good basis set is obtained when the fragments mutually overlap.[7] To calculate the electronic states in the desired spectral region (within 0.5 eV below the top of the valence band) with good accuracy, only one eigenstate (the HOMO state) of each fragment is needed. When the basis set is obtained, transfer and overlap integrals between basis states are calculated and subsequently, the Hamiltonian generalized eigenvalue problem is solved. These calculations can be done using parallel computer architectures, which saves a lot of computational time. A detailed description of the OFM can be found in Ref. 21.

In this work, the effect of polarons was not included. Previous DFT calculations of long straight polythiophene chains at zero temperature indicate that polaron binding energy is on the order of few meVs only and that it can be ignored.[35,36] However, it is more difficult to assess the role of polarons at finite temperature when thermal disorder is present in the material. Since the main goal of this work is to understand the effect of thermal disorder on wave function localisation and DOS, as well as the contributions from main and side chains to thermal disorder, polaronic effects were not considered.

Next, we discuss the appropriateness of LDA for the description of the localisation effects. The localisation effects that we observe essentially come from two effects: (i) variations of on-site energies of rings; (ii) variations in electronic coupling between the rings. The effect (i) comes mainly from disordered long range electrostatic potential that side chains, the rest of the main chain and other main chains produce on a certain ring. Within DFT, electrostatic potential is taken into account through the Hartree term in the Kohn-Sham equation, which is an exact term. Therefore, for the effect (i), the use of LDA in our calculation is not an issue. To check if LDA gives reliable values of electronic coupling (the effect (ii)),

we have performed the calculation of electronic energy levels of ten units long straight thiophene oligomer using either LDA or B3LYP functional for the same atomic configuration. These calculations have been performed using the NWChem code[37,38] and 6-31G basis set was used to represent the wave functions. We find that the spacing between energy levels calculated using these two functionals differs typically by 15 %. Since the spacing between energy levels of straight oligomers is proportional to electronic coupling between the rings, we conclude that possible uncertainties in electronic coupling calculated using LDA are on the order of 10-20% and such uncertainties are not expected to significantly affect the localisation lengths.

3 Results and discussion

The effects of thermal disorder in crystalline P3HT are investigated by examining 3 different types of structures: the structures with disorder in side chains, the structures with disorder in main chains and the structures with disorder in both side and main chains. In the first case, main chains are kept rigid during the MC simulation, while side chains are allowed to move freely. In the second case, side chains are removed (more precisely, replaced with a hydrogen atom) before the electronic structure calculations start, in order to isolate the effects of main chains disorder. In the case of structures with the presence of disorder in both main and side chains, the same atomic configurations are used as for the second case, but side chains are not removed in this case. To get sufficiently large statistics, for each of the investigated cases and for both aligned and shifted structures, 100 different realizations are generated. Each configuration contains 10 polymer chains stacked in the π-π direction, while each chain contains 10 rings. The total number of atoms in each configuration is 2520. For subsequent analysis only 10 highest states from each configuration are taken into account, since they cover a spectral range of about 0.5 eV below the HOMO level, which is the range of interest for the electrical transport properties. To analyse the effects of disorder, we calculate the DOS and the localisation length of hole states.

3.1 Density of electronic states

Densities of states obtained from the calculations are shown in Fig. 3. In the case of disorder in side chains in the aligned structure, DOS is nearly discrete, composed of several peaks (Fig. 3a). These peaks correspond to the peaks in the DOS of the ideal crystalline structure without any disorder. In the shifted structure, peaks are broader and overlap more than in the aligned structure, making DOS continuous (Fig. 3b). Thus, the effects of side chains disorder on DOS are more pronounced in the shifted structure than in the aligned. The

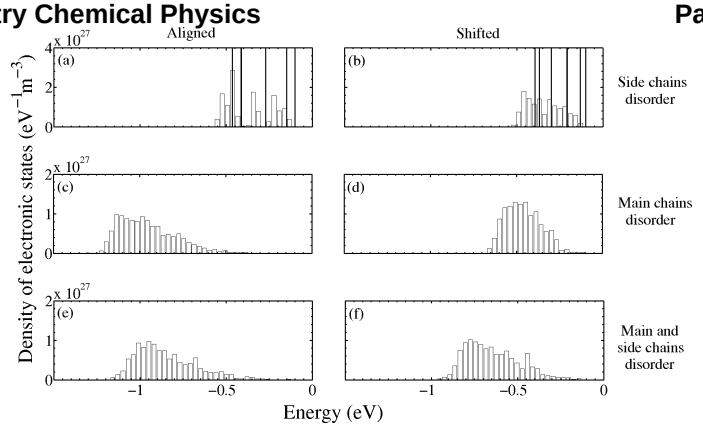

Fig. 3 DOS in the case of: (a) aligned structure with disorder in the side chains (bins) and ideal crystalline aligned structure (vertical lines); (b) shifted structure with disorder in the side chains (bins) and ideal crystalline aligned structure (vertical lines); (c) aligned structure with disorder in main chains and side chains omitted; (d) shifted structure with disorder in main chains and side chains omitted; (e) aligned structure with disorder in both side and main chains (f) shifted structure with disorder in both side and main chains.

difference in DOS for shifted and aligned structures can be explained by the difference in the spatial distribution of side chains in these two structures. In the aligned structure, side chains connected to the aligned thiophene rings from neighbouring chains in the π - π direction are at the same side of the main chains (chains denoted by 1 and 2 in Fig. 2a). On the other hand, in the shifted structure these side chains are at the opposite sides. The distance between nearest side chains in the shifted structure (chains denoted by 1 and 2 in Fig. 2b) is greater than in the aligned. Therefore, side chains in the shifted structure have more conformational freedom than in the aligned. This is evidenced by the distributions of the thiophene-side chain torsion angle for both structures, given in Fig. 4a and Fig. 4b. The distribution of thiophene-side chains torsion angles is significantly wider in the shifted structure, which results in higher degree of side chains disorder. This difference in morphology leads to the difference in the electronic structure.

In the structures with disordered main chains, DOS is continuous (Fig. 3c and Fig. 3d). In the case of aligned structures distribution of energies is significantly wider than in the shifted structure. Distributions of thiophene - thiophene torsion angles for the aligned and shifted structures are similar (Fig. 4c and Fig. 4d) and agree well with the results of Ref. 16. Therefore, the difference in the distribution of the energies is not caused by the shape of the chains. Electronic coupling between different chains is 0.11 eV in the ideal aligned structure and 0.07 eV in the ideal shifted structure. This substantial difference leads to the wider distribution of the energies in the

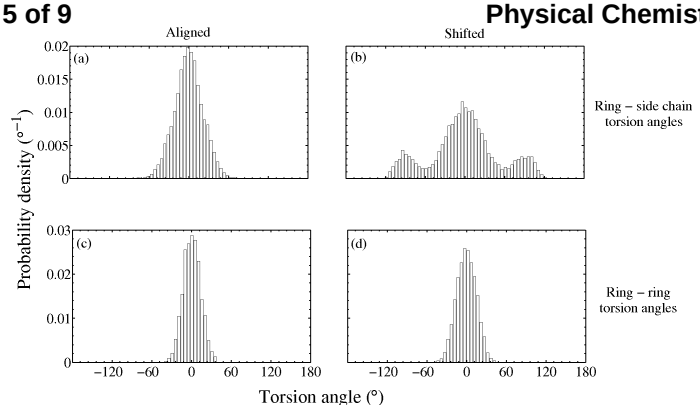

Fig. 4 Distribution of the: (a) thiophene-side chains torsion angles in the aligned structure; (b) thiophene-side chains torsion angles in the shifted structure; (c) thiophene-thiophene torsion angles in the aligned structure; (d) thiophene-thiophene torsion angles in the shifted structure. In panels (c) and (d) the angles are shifted by 180° for clarity. To exclude the effects of finite box dimension in the main chain direction, in (c), (d), (e) and (f) only torsion angles between rings in the middle of the chains are taken into account.

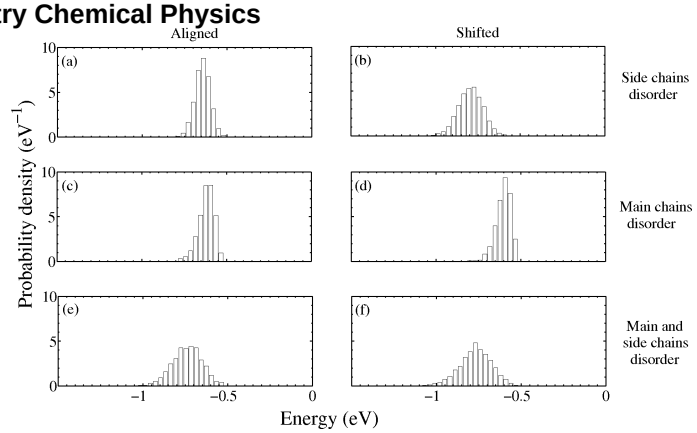

Fig. 5 Distribution of the diagonal elements of the Hamiltonian in: (a) aligned structure with disorder in side chains; (b) shifted structure with disorder in side chains; (c) aligned structure with disorder in main chains and side chains omitted; (d) shifted structure with disorder in main chains and side chains omitted; (e) aligned structure with disorder in both main and side chains and (f) shifted structure with disorder in both main and side chains. To exclude the effects of finite box dimension in the main chain direction, in (c), (d), (e) and (f) only trimers in the middle of the chains are taken into account.

aligned structure. When both main and side chains are disordered, the DOS is continuous (Fig. 3e and Fig. 3f) without any apparent difference between structures. This similarity in DOS can be explained by the effect of compensation between wider energy distribution in the shifted structure when only side chains are disordered and wider energy distribution in the aligned structure when only main chains are disordered.

Suitable measure of disorder in the system is the distribution of diagonal Hamiltonian elements given by $H_{ii} = \langle i \mid H \mid i \rangle$, where $\mid i \rangle$ are wave functions of trimers and H is the Hamiltonian of the system. Wave functions of the trimers are localised on the main chain and on the carbon atoms in the side chains closest to the thiophene rings. Consequently, if main chains of trimers are rigid, their wave functions and energies of HOMO levels will be equal. When only disorder in side chains is applied, difference between diagonal Hamiltonian elements arises only from variations in H, due to the variations in the electrostatics potential caused by side chains disorder. On the other hand, when disorder in main chains is present, variations in H_{ii} arises both form H and $\mid i \rangle$, since wave functions of trimers now differ significantly. Distributions of diagonal elements of the Hamiltonian are given in Fig. 5. As expected, distributions are widest in the case when both disorders are present (Fig. 5e and Fig. 5f). Having in mind the results for DOS presented above which suggest that disorder in main chains has more impact on the electronic structure of P3HT than disorder in side chains, one may find unexpected that distributions given in Fig. 5c and Fig. 5d are similar to the distributions given in Fig. 5a and Fig. 5b. Side chains have more conformational freedom than main chains, especially in the shifted structure. Therefore, their disorder affects the electrostatical potential more than disorder in main chains. When effects of disorder in main chains are isolated, side chains are removed and, consequently, variations of electrostatic potential are weaker than in the case of disorder in side chains, which leads to the weaker variations in H.

3.2 Wave function localisation

Wave functions of HOMO levels for 6 different cases are shown in Fig. 6. In the ideal crystalline structure the wave function of HOMO level (and any other level) is completely delocalised, as Bloch theory predicts. When the side chains disorder is partially applied, wave functions remain delocalised (Fig. 6a and Fig. 6b). They are not delocalised along the whole structure, as in the ideal structure. Delocalisation is broken both in the π-π stacking direction and in the main chain direction. On the other hand, wave functions of HOMO levels in the case of disorder in main chains are localised, both with and without side chains included (Fig. 6c - f). They are localised on 5 - 15 rings, usually on 2 neighbouring chains (as in Fig. 6c and Fig. 6e). Therefore, thermal disorder in the crystalline P3HT localises the wave function of HOMO level, as in the amorphous phase.[6,7]

To investigate the effects of disorder on the wave functions localisation more precisely, we calculate two localisation lengths for each state: localisation in the π-π stacking

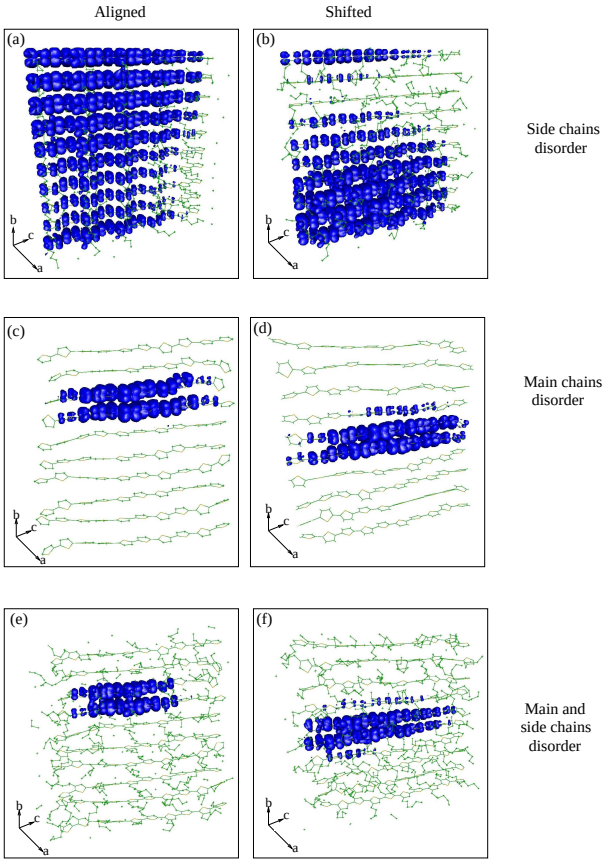

Fig. 6 Wave function moduli of the HOMO level of crystalline P3HT in the case of: (a) aligned structure with disorder in side chains; (b) shifted structure with disorder in side chains; (c) aligned structure with disorder in main chains and side chains omitted; (d) shifted structure with disorder in main chains and side chains omitted; (e) aligned structure with disorder in both side and main chains (f) shifted structure with disorder in both side and main chains. Isosurfaces correspond to the probability of finding a hole inside the surface of 90%.

direction L_b and localisation in the main chain direction L_c. If the wave functions are represented in the orthonormal basis set of well localised orbitals, the localisation length can be generally defined as $L = 1/\sum_m |d_m|^4$, where d_m are expansion coefficients of the wave functions in the orthonormal basis $|m\rangle$.[7] The basis set used in the OFM calculations is not orthonormal. The orthonormal basis set is constructed by transformation $|m\rangle = \sum_m T_{mi}|i\rangle$ with transformation matrix $T = (S^{-1/2})^*$, where S is the original overlap matrix and $|i\rangle$ are original basis wave functions. Expansion coefficients of the orthonormal basis set are related to the original coefficients c_i via $d_m = \sum_i (S^{1/2})_{mi} c_i$. For the orthonormal basis set the condition $\sum_m |d_m|^2 = 1$ is satisfied. In our case, this sum can be divided into two sums, one over different chains and other over rings in one chain: $\sum_{i=1}^{N_c} \sum_{j=1}^{N_m} |\beta_{ij}|^2 = 1$, where N_c and N_m are the number of chains and the number of rings within one chain, respectively. Following the general definition of the localisation length, L_b is defined as $L_b = 1/\sum_i \left|\beta_i'\right|^4$, where $\left|\beta_i'\right|^2 = \sum_{j=1}^{N_m} |\beta_{ij}|^2$. Similarly, L_c is defined as $L_c = 1/\sum_j \left|\beta_j''\right|^4$, where $\left|\beta_j''\right|^2 = \sum_{i=1}^{N_c} |\beta_{ij}|^2$.

Plots of the dependence of L_b on energy of the electronic states are shown in Fig. 7. In the ideal crystalline structure (both aligned and shifted), L_b of the HOMO level is equal to the number of chains, which is 10 in this case. Lower states in the ideal structure have L_b either 6.67 or 10. In the case of the aligned structure with disordered side chains (Fig. 7a), the values of L_b for HOMO level vary from 4 to 10. Other states have L_b which is around the value of L_b in the ideal structure. In the case of the shifted structure, distribution of the energies of states is wider then in the aligned. Consequently, it is difficult to isolate the values of L_b for HOMO levels from Fig. 7b. Looking into the range of 0.2 eV below the highest energy, value of L_b is between 3 and 6, which is lower than the values of L_b in aligned structures. Therefore, wave functions of HOMO levels are more localised in the shifted structure than in the aligned. In all remaining cases (Fig. 7c-f) we get qualitatively similar results. Values of L_b for the highest occupied states are low, they take values from 2 to 4 chains. States with lower energies have wider distributions of L_b, suggesting that delocalised states exist. Shape of the plot of L_b is similar to the plot of the hole localisation length of the amorphous P3HT, given in Ref. 7.

Results for L_c are similar to the results for L_b. Minimal value for L_c when both side and main chains are disordered is 3. Electronic coupling is stronger in the main chain direction than in the π-π stacking direction and therefore localisation in the π-π stacking direction is stronger than in the chain direction. It is interesting to note that the highest states in the valence band are typically localised on 2 neighbouring chains when main chains are disordered. State will be localised on

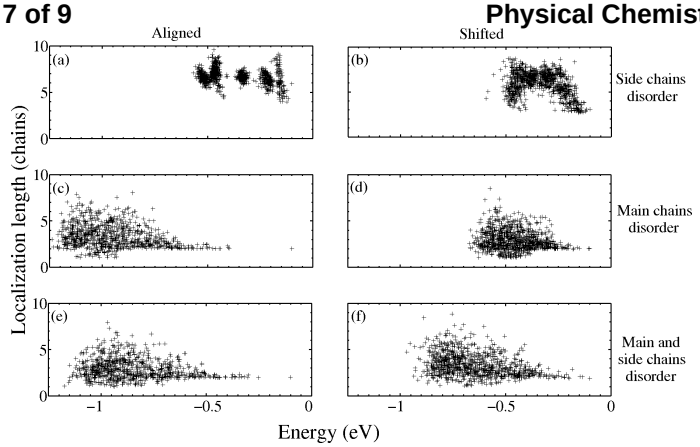

Fig. 7 Dependence of L_b on the energy of the electronic state in the case of: aligned structure with disorder in the side chains; (b) shifted structure with disorder in the side chains; (c) aligned structure with disorder in main chains and side chains omitted; (d) shifted structure with disorder in main chains and side chains omitted; (e) aligned structure with disorder in both side and main chains (f) shifted structure with disorder in both side and main chains.

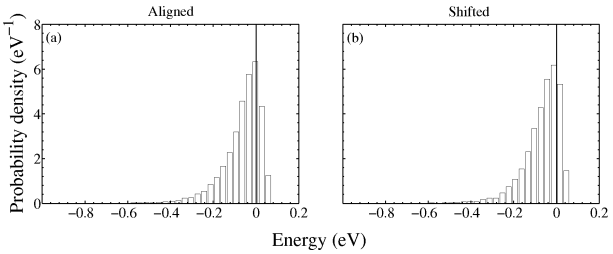

Fig. 8 Distribution of difference between electronic coupling between chains and variations of diagonal Hamiltonian elements in the case of: (a) aligned and (b) shifted structure.

two chains if the electronic coupling $t_{mn} = \langle m|H|n\rangle$ between orbitals m and n from different chains is greater then variations of the diagonal Hamiltonian elements. The distributions of the quantity $d = t_{mn} - |H_{mm} - H_{nn}|$ are given in Fig. 8. Since d takes positive values as well, existence of strong coupling between chains is confirmed, which explains localisation on two neighbouring chains.

Total localisation length can be found using general definition previously given. Plots of its dependence on energy of the states is given in Fig. 9. For the highest states, when main chains are disordered, it takes values from 5 to 15 rings (Fig. 9c-f). These values are slightly higher than the values of the localisation length of highest states in the valence band of amorphous P3HT, which is around 5.[7] This difference is expected, since crystalline P3HT, despite high degree of disorder, is still more ordered than amorphous. In the sense of the hole localization length, effects of disorder in crystalline and amorphous P3HT are similar. Delocalised states (localised on more than 10 rings) start to appear only few hundreds of meV below the top of the valence band. This is in agreement with findings presented in Ref. 17 where DOS and localization length in PBTTT are calculated. Results for the carrier localization orbital density of HOMO levels of crystalline P3HT at 300 K, given in Ref. 15, indicate the presence of both localised (4-10 rings) and weakly (more than 10 rings) localised states. These calculations were performed without alkyl side chains and for isolated main chains. We obtain qualitatively the same results for L_c, since we find states localised on few rings within a chain and states that are extended over the entire chain. To conclude, our findings agree with previous that wave functions of the highest states in the valence band are localised and that delocalised (or weakly localised) states also exist below these states.

Results for total localization length and L_b are qualitatively similar for the structures with isolated disorder in main chains and with both disorder in main and side chains. Nevertheless, side chains have a significant quantitative effect on electronic properties. This can be seen by comparing the DOS (Fig. 3c vs. Fig. 3e and Fig. 3d vs. Fig. 3f), localization length (Fig. 9c vs. Fig. 9e and Fig. 9d vs. Fig. 9f) and on-site Hamiltonian elements (Fig. 5c vs. Fig. 5e and Fig. 5d vs. Fig. 5f). By comparing the figures one can also see that the effect of side chains disorder is stronger in the shifted than in the aligned structure which happens due to their larger conformational freedom in the shifted structure, as discussed in Sec 3.1. Therefore, to obtain reliable results, side chains should be included into the calculations.

3.3 Consequences for electrical transport

We now discuss the consequences of our findings about thermal disorder on electrical properties of the material. In small molecule based organic crystals (SMOCs) the effects of thermal disorder[14] were used to explain the temperature dependence of the mobility where the mobility that decreases with increasing temperature is typically observed. On the other hand, all mobility measurements of P3HT, even for highest quality ordered samples, yield a thermally activated temperature dependence.

Our results suggest that in ordered P3HT there is a spectral region within first 200 meV below the top of the valence band with electronic states localised to just a few rings. In a combined molecular dynamics - electronic structure study in Ref. 15 such states were found to be persistently localised in the sense that their position does not vary over the time on the order of few nanoseconds. Below the spectral region with localised states, there is a region where both localised and delocalised states exist. It is well understood that the spatial

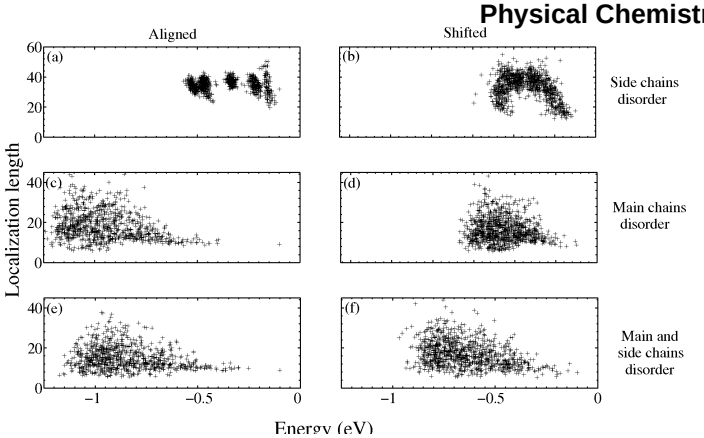

Fig. 9 Dependence of the total localization length on the energy of the electronic state in the case of:(a) aligned structure with disorder in the side chains; (b) shifted structure with disorder in the side chains; (c) aligned structure with disorder in main chains and side chains omitted; (d) shifted structure with disorder in main chains and side chains omitted; (e) aligned structure with disorder in both side and main chains (f) shifted structure with disorder in both side and main chains.

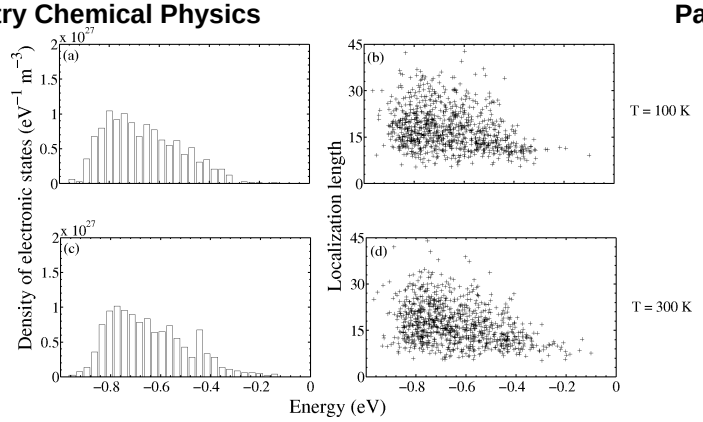

Fig. 10 (a) DOS of the shifted structure with disorder in main and side chains at 100 K. (b) Dependence of the total localization length on the energy of the electronic state of the shifted structure with disorder in main and side chains at 100 K. (c) DOS of the shifted structure with disorder in main and side chains at 300 K. (d) Dependence of the total localization length on the energy of the electronic state of the shifted structure with disorder in main and side chains at 300 K.

and energetic distribution of electronic states that we obtained leads to thermally-activated transport; at low temperature most carriers populate localised states at the top of the valence band which yield low mobility, while at higher temperatures less localised or delocalised states become more populated and the transport is much better then.[39]

However, what is the main difference between polymers and SMOCs where a different temperature dependence of mobility is observed? In SMOCs, thermal disorder leads to localised electronic states, as well. However, the spectral region where these states exist is much narrower. For example, in Ref. 13 the spectral region with strongly localised states has the width of approximately $0.2t$, where t is the electronic coupling transfer integral between two neighbouring molecules (which is typically on the order of 100 meV in SMOCs). In Ref. 10 this range is equally narrow and is comparable to or even smaller than thermal energy k_BT at room temperature. For this reason, thermally activated behaviour is not observed in SMOCs.

The comparison between the effects of thermal disorder in ordered polymers and SMOCs illustrates the dual role of temperature when thermal disorder and transport properties are concerned. The temperature acts on the one hand to create well localised states and on the other hand to promote the carriers from such localised states to delocalised states with better transport. In SMOCs higher temperatures lead to better localization of the states and consequently to a smaller mobility. On the other hand, in ordered P3HT polymers, in the range of temperatures from 100K to 300K, the temperature has a weak effect on the DOS and on the dependence of localization length on energy. This conclusion was obtained from the comparison of these two quantities at 100K and 300K, presented in Fig. 10. A weak effect of temperature on the degree of localization was also shown in Ref. 15 (Table I). Therefore, the temperature dependence of mobility in ordered polymers originates from thermal activation of carriers from localised states to delocalised or less localised states with better transport. While we show that the effects of thermal disorder alone lead to thermally activated mobility, this does not necessarily imply that they are the dominant cause of thermally activated mobility observed in realistic samples. Various imperfections of chemical or structural nature produce traps where carriers can be localised and these can also lead to thermally activated mobility.

4 Conclusion

In this work the effects of thermal disorder on the electronic structure of crystalline P3HT were investigated. The influence of side chains and main chains on the thermal disorder were investigated separately for the first time. The main conclusions from the obtained results can be summarized as follows. The disorder in side chains has a significant effect on the electronic structure of P3HT. The effect is more pronounced in the shifted structure than in the aligned, due to higher conformational freedom of side chains. The disorder in main chains has a strong effect on the electronic structure, leading to the lo-

calization of HOMO levels wave functions to few rings only. Such a degree of localization is similar to the localisation in amorphous P3HT and it is a possible cause of thermally activated mobility that is typically observed in ordered polymers.

5 Acknowledgment

This work was supported by a European Community FP7 Marie Curie Career Integration Grant (ELECTROMAT), the Serbian Ministry of Education, Science and Technological Development (Project ON171017) and FP7 projects (PRACE-3IP, HP-SEE[40] and EGI-InSPIRE).

References

1 R. H. Friend, R. W. Gymer, A. B. Holmes, J. H. Burroughes, R. N. Marks and et al, *Nature*, 1999, **397**, 121–128.
2 J. H. Burroughes, D. D. C. Bradley, A. R. Brown, R. N. Marks, K. Mackay, R. H. Friend, P. L. Burns and A. B. Holmes, *Nature*, 1990, **347**, 539–541.
3 V. L. Colvin, M. C. Schlamp and A. P. Alivisatos, *Nature*, 1994, **370**, 354–357.
4 A. Dodabalapur, L. Torsi and H. E. Katz, *Science*, 1995, **268**, 270–271.
5 G. Li, V. Shrotriya, J. S. Huang, Y. Yao, T. Moriarty, K. Emery and Y. Yang, *Nat. Mater.*, 2005, **4**, 864.
6 N. Vukmirović and L. W. Wang, *J. Phys. Chem. B*, 2009, **113**, 409–415.
7 N. Vukmirović and L.-W. Wang, *J. Phys. Chem. B*, 2011, **115**, 1792–1797.
8 T. Vehoff, B. Baumeier, A. Troisi and D. Andrienko, *J. Am. Chem. Soc.*, 2010, **132**, 11702–11708.
9 A. Troisi and D. L. Cheung, *J. Chem. Phys.*, 2009, **131**, 014703.
10 A. Troisi, *J. Chem. Phys.*, 2011, **134**, 034702.
11 J. Böhlin, M. Linares and S. Stafström, *Phys. Rev. B*, 2011, **83**, 085209.
12 Y. Yao, W. Si, X. Hou and C.-Q. Wu, *J. Chem. Phys.*, 2012, **136**, 234106.
13 S. Fratini and S. Ciuchi, *Phys. Rev. Lett.*, 2009, **103**, 266601.
14 A. Troisi and G. Orlandi, *Phys. Rev. Lett.*, 2006, **96**, 086601.
15 D. L. Cheung, D. P. McMahon and A. Troisi, *J. Am. Chem. Soc.*, 2009, **131**, 11179–11186.
16 D. P. McMahon, D. L. Cheung, L. Goris, J. Dacuna, A. Salleo and A. Troisi, *J. Phys. Chem. C*, 2011, **115**, 19386–19393.
17 T. Liu and A. Troisi, *Adv. Funct. Mater.*, 2013, **24**, 925–933.
18 M. Allen and D. J. Tildesley, *Computer Simulation of Liquids*, Clarendon Press, Oxford Science Publications, New York, USA, 1987.
19 N. Vukmirović and L. W. Wang, *J. Chem. Phys.*, 2008, **128**, 121102.
20 M. Mladenovic, N. Vukmirovic and I. Stankovic, *J. Phys. Chem. C*, 2013, **117**, 15741–15748.
21 N. Vukmirovic and L.-W. Wang, *J. Chem. Phys.*, 2011, **134**, 094119.
22 D. L. Cheung, D. P. McMahon and A. Troisi, *J. Phys. Chem. B*, 2009, **113**, 9393–9401.
23 O. Alexiadis and V. G. Mavrantzas, *Macromolecules*, 2013, **46**, 2450–2467.
24 S. Dag and L.-W. Wang, *J. Phys. Chem. B*, 2010, **114**, 5997–6000.
25 W. Xie, Y. Y. Sun, S. B. Zhang and J. E. Northrup, *Phys. Rev. B*, 2011, **83**, 184117.
26 C. Poelking and D. Andrienko, *Macromolecules*, 2013, **46**, 8941–8956.
27 R. S. Bhatta, Y. Y. Yimer, D. S. Perry and M. Tsige, *J. Phys. Chem. B*, 2013, **117**, 10035–10045.
28 M. Moreno, M. Casalegno, G. Raos, S. V. Meille and R. Po, *J. Phys. Chem. B*, 2010, **114**, 1591–1602.
29 T. J. Prosa, M. J. Winokur, J. Moulton, P. Smith and A. J. Heeger, *Macromolecules*, 1992, **25**, 4364–4372.
30 R. Colle, G. Grosso, A. Ronzani and C. M. Zicovich-Wilson, *Phys. Status Solidi B*, 2011, **248**, 1360–1368.
31 N. Kayunkid, S. Uttiya and M. Brinkmann, *Macromolecules*, 2010, **43**, 4961–4967.
32 A. Maillard and A. Rochefort, *Phys. Rev. B*, 2009, **79**, 115207.
33 W. L. Jorgensen, D. S. Maxwell and J. Tirado-Rives, *J. Am. Chem. Soc.*, 1996, **118**, 11225–11236.
34 R. G. Parr and W. Yang, *Density-Functional Theory of Atoms and Molecules*, Oxford University Press, New York, USA, 1989.
35 K. D. Meisel, H. Vocks and P. A. Bobbert, *Phys. Rev. B*, 2005, **71**, 205206.
36 S. Zade and M. Bendikov, *Chemistry - A European Journal*, 2008, **14**, 6734–6741.
37 E. J. Bylaska, W. A. de Jong, N. Govind, K. Kowalski, T. P. Straatsma, M. Valiev, D. Wang, E. Apra, T. L. Windus, J. Hammond, P. Nichols, S. Hirata, M. T. Hackler, Y. Zhao, P.-D. Fan, R. J. Harrison, M. Dupuis, D. M. A. Smith, J. Nieplocha, V. Tipparaju, M. Krishnan, Q. Wu, T. V. Voorhis, A. A. Auer, M. Nooijen, E. Brown, G. Cisneros, G. I. Fann, H. Fruchtl, J. Garza, K. Hirao, R. Kendall, J. A. Nichols, K. Tsemekhman, K. Wolinski, J. Anchell, D. Bernholdt, P. Borowski, T. Clark, D. Clerc, H. Dachsel, M. Deegan, K. Dyall, D. Elwood, E. Glendening, M. Gutowski, A. Hess, J. Jaffe, B. Johnson, J. Ju, R. Kobayashi, R. Kutteh, Z. Lin, R. Littlefield, X. Long, B. Meng, T. Nakajima, S. Niu, L. Pollack, M. Rosing, G. Sandrone, M. Stave, H. Taylor, G. Thomas, J. van Lenthe, A. Wong and Z. Zhang, *NWChem, A Computational Chemistry Package for Parallel Computers, Version 5.1*, Pacific Northwest National Laboratory, Richland, Washington 99352-0999, USA, 2007.
38 M. Valiev, E. Bylaska, N. Govind, K. Kowalski, T. Straatsma, H. V. Dam, D. Wang, J. Nieplocha, E. Apra, T. Windus and W. de Jong, *Comp. Phys. Comm.*, 2010, **181**, 1477.
39 N. F. Mott and E. A. Davis, *Electronic Processes in Non-Crystalline Materials*, Clarendon Press, New York, USA, 1979.
40 This work makes use of results produced by the High-Performance Computing Infrastructure for South East Europe's Research Communities (HP-SEE), a project co-funded by the European Commission (under contract number 261499) through the Seventh Framework Programme. HP-SEE involves and addresses specific needs of a number of new multidisciplinary international scientific communities and thus stimulates the use and expansion of the emerging new regional HPC infrastructure and its services. Full information is available at: `http://www.hp-see.eu/`.